

## Proximity-induced Shiba states in a molecular junction

Joshua O. Island,<sup>1, a)</sup> Rocco Gaudenzi,<sup>1</sup> Joeri de Bruijckere,<sup>1</sup> Enrique Burzurí,<sup>1</sup>  
 Carlos Franco,<sup>2</sup> Marta Mas-Torrent,<sup>2</sup> Concepció Rovira,<sup>2</sup> Jaume Veciana,<sup>2</sup> Teun M.  
 Klapwijk,<sup>1, 3</sup> Ramón Aguado,<sup>4</sup> and Herre S. J. van der Zant<sup>1</sup>

<sup>1)</sup>*Kavli Institute of Nanoscience, Delft University of Technology, Lorentzweg 1, 2628 CJ Delft, The Netherlands.*

<sup>2)</sup>*Institut de Ciència de Materials de Barcelona (ICMAB-CSIC) and CIBER-BBN, Campus de la UAB, 08193, Bellaterra, Spain.*

<sup>3)</sup>*Physics Department, Moscow State Pedagogical University, Moscow 119991, Russia.*

<sup>4)</sup>*Instituto de Ciencia de Materiales de Madrid, Consejo Superior de Investigaciones Científicas (ICMM-CSIC), Sor Juana Inés de la Cruz 3, 28049 Madrid, Spain.*

Superconductors containing magnetic impurities exhibit intriguing phenomena derived from the competition between Cooper pairing and Kondo screening. At the heart of this competition are the Yu-Shiba-Rusinov (Shiba) states which arise from the pair breaking effects a magnetic impurity has on a superconducting host. Hybrid superconductor-molecular junctions offer unique access to these states but the added complexity in fabricating such devices has kept their exploration to a minimum. Here, we report on the successful integration of a model spin 1/2 impurity, in the form of a neutral and stable all organic radical molecule, in proximity-induced superconducting break-junctions. Our measurements reveal excitations which are characteristic of a spin-induced Shiba state due to the radical's unpaired spin strongly coupled to a superconductor. By virtue of a variable molecule-electrode coupling, we access both the singlet and doublet ground states of the hybrid system which give rise to the doublet and singlet Shiba excited states, respectively. Our results show that Shiba states are a robust feature of the interaction between a paramagnetic impurity and a proximity-induced superconductor where the excited state is mediated by correlated electron-hole (Andreev) pairs instead of Cooper pairs.

---

<sup>a)</sup>Electronic mail: j.o.island@tudelft.nl

A quantum dot (QD) or impurity coupled to a superconductor constitutes a rich physical system in which many-body effects compete for the ground state<sup>1–9</sup>. The ground state can take the form of a BCS-like singlet, a spin degenerate doublet, or a Kondo-like singlet depending on the relative strengths of the characteristic energies of the competing phenomena (charging energy,  $U$ , superconducting gap,  $\Delta$ , Kondo energy,  $T_K$ ). For weak Coulomb interaction ( $U \ll \Delta$ ), the BCS singlet, composed of the superposition of unoccupied and doubly occupied states of the dot, prevails. Subgap excitations of this ground state are the well-known Andreev bound states. This regime has been explored in carbon nanotube<sup>10,11</sup> and nanowire<sup>12,13</sup> devices where  $\Delta$  can be large enough relative to  $U$  to allow the BCS superposition state. For larger charging energy however, the doublet becomes the energetically favored ground state (at temperatures above  $T_K$ ) and a competition between Kondo screening and Cooper pairing sets in at temperatures below  $T_K$ <sup>8,14</sup>. For weak Kondo energy ( $T_K \ll \Delta$ ) the ground state is the degenerate doublet as screening is incomplete due to a lack of quasiparticles at the Fermi level. For strong Kondo energy ( $T_K \gg \Delta$ ), quasiparticles screen the spin and the Kondo singlet becomes the ground state. Excitations on top of these ground states are the Yu-Shiba-Rusinov (or simply Shiba) states<sup>15–18</sup>. First experimentally observed in tunneling spectra of magnetic adatoms absorbed on Nb<sup>19</sup>, these states were recently shown to lead to topological Shiba bands required for the observation of Majorana end modes in atomic chains adsorbed on a superconducting surface<sup>20–22</sup>.

Besides early tunneling experiments on Kondo alloys producing conventional Shiba bands<sup>23</sup>, the great majority of investigations of superconductor-QD systems are with magnetic impurities<sup>2,7,19,24</sup>, nanowires<sup>3,4</sup> or nanotubes<sup>25–27</sup> coupled directly to a bulk superconductor. In these systems the singlet Shiba excited state is created by breaking a Cooper pair which allows a quasiparticle to pair with the localized spin in the quantized system. A similar interaction may occur through proximity induced superconductivity but has not been explored and requires attention as proposals and investigations of Majorana bound states engineered through proximity induced systems grow<sup>12,28–33</sup>.

The hybrid superconductor-molecule device grants a unique exploration of the superconductor-QD phase diagram as the energy spacing between molecular orbitals of a molecule is typically orders of magnitude larger than the other energy scales completely suppressing the formation of the BCS-like singlet ground state and offering investigation of the large- $U$  regime. The added difficulty in fabricating such devices has limited their investigation to only a

few studies<sup>34,35</sup>. Additionally, direct contact to a superconductor leads to only weak coupling (relatively small  $\Gamma$ ) leaving access to the Kondo regime (and competing phenomena) unattainable<sup>34</sup>. Instead, gold can be used as an intermediate material allowing stronger coupling through the sulfur-gold bond but is not superconducting itself and thus requires exploitation of the proximity effect.

Here we report on investigations of the large- $U$  regime of the superconductor-QD system and the observation of Shiba states in a completely proximitized superconducting junction hosting a model spin 1/2 impurity. As opposed to direct coupling to a bulk superconductor with a phase coherent condensate giving rise to spin induced Shiba states, Shiba states in our system are supported by correlated electron-hole (Andreev) pairs. Fig. 1(a) depicts this situation in which a magnetic impurity (in our case a molecule with an unpaired spin at its center signified by a red circle) on the left side is tunnel coupled to a proximity-induced superconductor on the right side. The proximity effect in the gold is mediated by the well-known Andreev reflection process that occurs at the interface between the normal metal (gold region) and the superconductor (blue region) giving rise to Andreev pairs in the gold leads<sup>36</sup> which can interact with the molecule through an exchange coupling. As a result of a variable molecule-electrode coupling for different devices, we access both the singlet and doublet ground states (and their corresponding Shiba excited states) of the large- $U$  superconductor-QD phase diagram. We further corroborate these results through calculations based on the Anderson impurity model while taking into account the proximity induced nature of the gold electrodes.

As a prototypical spin 1/2 impurity for this study, we have judiciously selected a neutral and stable all organic radical (polychlorotriphenylmethyl, PTM) which we have shown produces a robust Kondo effect in gold break-junctions<sup>37</sup>. The chemical structure of the molecule is shown on the left side of fig. 1(a). Three chlorinated phenyl rings are connected to the central carbon atom through  $sp^2$  hybridization<sup>38</sup>. A single unpaired electron, giving the molecule an intrinsic paramagnetic ground state, is mainly localized at the central carbon atom and protected from the environment by the more bulky chlorine atoms. This protection gives the radical its high chemical and thermal stability. Additionally, this stability has been shown to result in Kondo correlations at low temperatures in gold break junctions which are stable against mechanical and electrostatic variations<sup>37</sup>. Density functional theory (DFT) calculations show that the Fermi energy (with gold electrodes) of the molecule sits within a

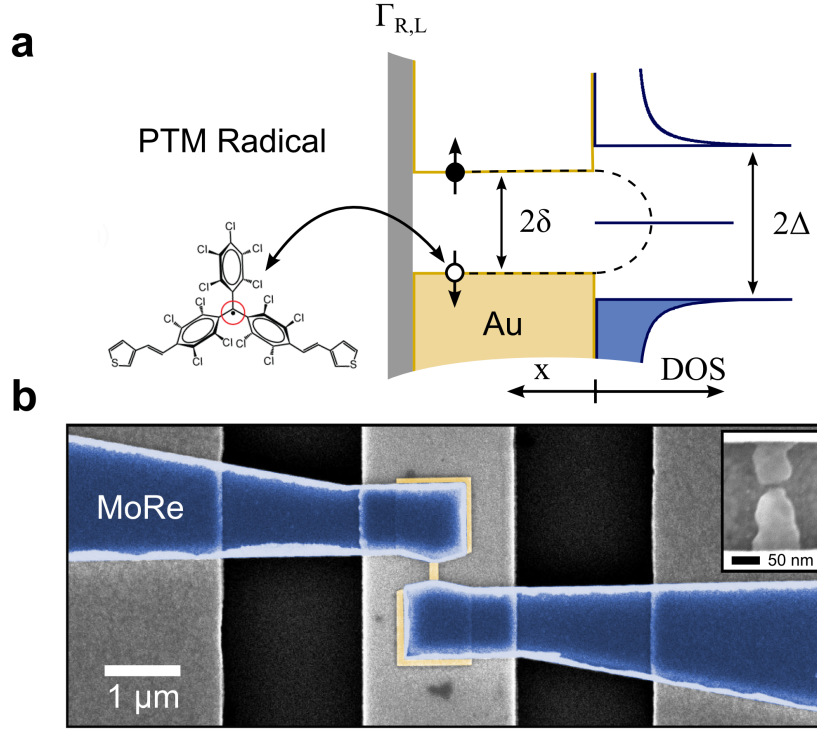


FIG. 1. **Proximity induced interaction with an all organic radical molecule and device design.** (a) Schematic representation of a radical molecule coupled to a proximity induced superconducting gold electrode. The red circle represents the unpaired spin at the center of the molecule. (b) False-colored scanning electron microscopy (SEM) image of a lithographically identical junction with superconducting electrodes colored blue and gold nanowire colored gold. The inset shows a SEM image of an electromigrated junction after measurement, scale bar 50 nm.

sizable energy gap (2 eV) between the singly occupied molecular orbital (SOMO) and the lowest unoccupied molecular orbital (LUMO) creating a stable electronic configuration with a large "charging energy" in the ground state. This is further verified by the absence of resonant transport at low bias in the whole range of gate voltages that can be applied in our electromigrated break junctions<sup>37</sup>. This makes the PTM radical an ideal molecule to explore the large  $U$  limit of the superconductor-QD phase diagram which favors Shiba excited states for both the singlet and doublet ground states.



## I. DEVICE DESIGN

The junction fabrication and characterization has been detailed in Refs.<sup>39,40</sup> which we briefly summarize here. Fig. 1(b) shows a false colored scanning electron microscopy (SEM) image of a representative junction. The blue colored electrodes are the bulk superconducting banks created by sputtering molybdenum-rhenium (60/40,  $T_c \approx 8.5K$ ). The gold colored nanowire and contact pads are created by electron-beam evaporation of gold (thickness, 12 nm). The gray vertical strip under the junction is a  $\text{AlO}_x/\text{AuPd}$  back gate which can be used to electrostatically gate the junction. A combination of electromigration and a self-breaking technique is used to open a nanogap in the gold nanowire. The inset shows an SEM image of a typical nanogap.

Several empty nanogaps are measured at low temperatures in order to characterize the superconducting proximity effect in the gold electrodes without molecules. In fig. 2(a) we show the low temperature (100 mK) differential conductance ( $dI/dV_b$ ) as a function of voltage bias ( $V_b$ ) for an empty junction (no molecule). The two conductance peaks at voltages of  $\approx \pm 1.6$  mV signal the overlap of the induced quasiparticle peaks in the two gold leads (see schematic in fig. 2(b)) and gives us a rough estimate of the induced mini-gap. A mini-gap ( $\delta$ , see fig. 1(a)) exists in the proximity-induced superconductor with a magnitude related to the Thouless energy,  $E_{th} = \hbar D/L^2$ , where  $D = 0.026$  m<sup>2</sup>/s is the diffusion constant for gold<sup>41</sup> and  $L$  is the electrode length<sup>42</sup>. If we assume a symmetric left and right gold electrode with a tunnel barrier in between, the length of each electrode is  $L \approx 140$  nm. This gives an estimate of  $\delta = 0.87$  meV which agrees roughly with the value obtained from fig. 2(a),  $\delta \approx 0.8$  meV. The position of the nanogap depends on the electromigration process and is not always symmetrically created at the center of the nanoribbon which leads to asymmetric proximity induced density of states (DOS) (see Supporting Information for details). As opposed to coupling directly to the bulk and having a BCS like DOS, our gold leads offer external tuning of the induced gap through application of a magnetic field. This allows *in-situ* tuning of  $\delta$  relative to the Kondo energy,  $T_K$ , and exploration of the phase transition between the singlet and doublet ground states.

In order to carry out measurements on the PTM molecule, a solution of molecules (concentration 1 mM) is drop-cast onto an array of 24 junctions before electromigration. After the electromigration and self-breaking of all junctions, the solution is evaporated leaving

behind roughly a monolayer of molecules and the sample is cooled down in a dilution refrigerator (base temperature 100 mK). All low temperature measurements are performed using a two-terminal voltage bias and numerical differentiation of the measured current/applied voltage to obtain the differential conductance. Detailed measurements were performed on 7 junctions (labeled A through G, see Supporting Information for an overview).

## II. THE NORMAL STATE

We now turn to the low temperature characteristics of our radical molecular junctions where we first show the results for the normal-state measurements. By applying a small finite perpendicular magnetic field (200 mT, directed out of the page in fig. 1(b)) to the junctions, the proximity effect in the normal leads can be completely suppressed. The curve in the inset of fig. 2(c) shows the differential conductance ( $dI/dV_b$ ) as a function of bias voltage in the normal state for device C. A zero-bias Kondo peak is observed which closely resembles measurements of the same molecule in all-gold junctions<sup>37</sup>. This peak is characterized as a function of temperatures up to 4 K (fig. 2(c)) and magnetic fields up to 8 T (fig. 2(d)). We observe the typical exponential decrease of the Kondo peak height with increasing temperature and its splitting in high magnetic fields. From the temperature dependence of the peak height we estimate a Kondo temperature of 4.4 K and from the splitting we estimate a g-factor of 2.4, all consistent with Kondo correlations observed in all-gold junctions. As reported previously<sup>37</sup>, we also observe little modulation of the peak in the normal state with electrostatic gating due to the sizable SOMO-LUMO gap (see Supporting Information).

From the linear conductance we furthermore estimate the asymmetry in the coupling ( $\Gamma_L, \Gamma_R$ ) to the leads using<sup>43</sup>:

$$G = \frac{2e^2}{h} \frac{4\Gamma_L\Gamma_R}{(\Gamma_L + \Gamma_R)^2} f(T/T_K) + G_b, \quad (1)$$

where  $f(T/T_K) = [1 + T^2/T_K^2(2^{1/s} - 1)]^{-s}$  with  $s = 0.22$  the expected value from numerical renormalization group theory for spin 1/2.<sup>44</sup> From Equation 1 we find an asymmetry of  $\Gamma_L/\Gamma_R \approx 5 \times 10^{-4}$ . This asymmetry is predominant in electromigrated junctions due to the random orientation of the molecule in the nanogap resulting in strongly different coupling strengths to the left and right electrodes.

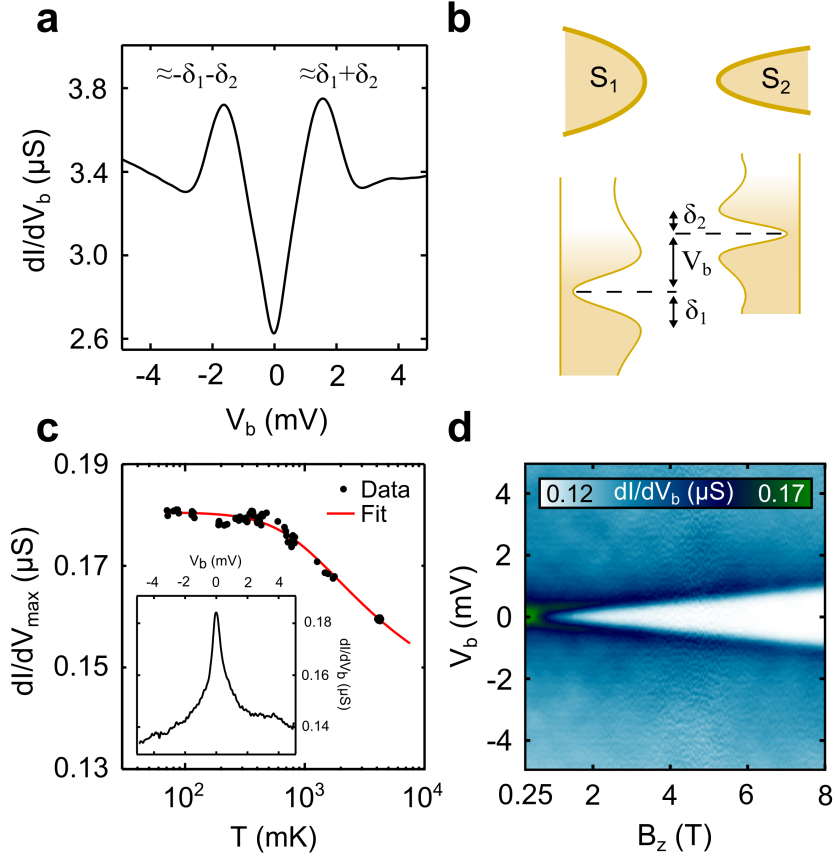


FIG. 2. **Low temperature characterizations of an empty junction and a molecular junction in the normal state.** (a) Low temperature (100 mK) measurement of the differential conductance ( $dI/dV$ ) as a function of voltage bias ( $V_b$ ) of an empty gap. (b) Schematic representation of the asymmetry in the proximity induced gaps of the left and right leads. (c)  $dI/dV$  vs.  $V_b$  showing the Kondo peak in the normal state (200 mT). The inset shows the temperature dependence which corresponds to a Kondo temperature of 4.4 K. (d)  $dI/dV$  as a function of  $V_b$  and magnetic field showing the splitting of the Kondo peak.

### III. THE SUPERCONDUCTING STATE

Moving now to the characteristics in the superconducting state, the black curve in fig. 3(a) shows the differential conductance as a function of voltage bias in the superconducting state ( $B = 0$  T) for device D. The red curve in the same panel is the measurement in the normal state ( $B = 200$  mT) showing the zero bias peak arising from the Kondo effect discussed previously. In the superconducting state two peaks are discernible, symmetric

in bias, accompanied by side dips at higher bias which are qualitatively distinctive from the empty junction curves in fig. 2(a) and in the Supporting Information. These peaks signal excitations of the coupled superconductor-QD system and have been shown to be associated with (multiple) Andreev reflections (MAR) and spin induced Yu-Shiba-Rusniov states. Conductance peaks due to MAR however are not accompanied by side dips and become less probable as the asymmetry between the left and right leads is increased<sup>3,25</sup>. Asymmetries of  $\Gamma_L/\Gamma_R \approx 10^{-2} - 10^{-3}$  in nanowire experiments are enough to completely suppress MAR contributions<sup>3</sup>. With the built in high asymmetry of the couplings and given the spin 1/2 Kondo effect in the normal state, a natural explanation for the excitation peaks in our hybrid molecular devices is that they originate from spin induced Shiba states.

Figure 3(c) shows a schematic of the coupling situation and density of states. The blue colored electrode and corresponding DOS represent the hybridization of the radical with the more strongly coupled electrode resulting in Shiba excited states. Microscopically, these states arise from the interaction of Andreev pairs at finite energy in the proximity-induced lead and the unpaired spin of the radical molecule. The weakly coupled gold lead on the right side essentially probes the hybridization of the molecule with the left electrode. This results in conductance peaks in fig. 3(a) at energies of  $\pm(E_b + \delta_2)$  where  $E_b$  is the excited state energy and  $\delta_2$  is the proximity-induced gap of the probe electrode. In addition to these peaks, side shoulders are visible at lower bias voltage which we interpret as Shiba replicas. Shiba replicas are visible for a sufficient density of quasiparticles in the mini-gap of the probe electrode which is reasonable considering the soft proximity-induced gap of our empty junctions (see fig. 2(a)). With an increase in temperature we furthermore observe the emergence of an anomalous zero-bias peak (dashed curve in Fig. 2(a)) which we interpret as a mini-Kondo due to increased quasiparticle filling (see Supporting Information for a discussion).

A comparison of the characteristic energies ( $\delta_{avg}$  vs.  $k_B T_K$ ) for device D allows us to determine the ground state of the coupled system. The edge of the dips in fig. 3(a) roughly correspond to  $\delta_1 + \delta_2$  from which we calculate an average induced gap of  $\delta_{avg} = (\delta_1 + \delta_2)/2 = 0.8$  meV. Compared with the Kondo energy extracted from the normal state temperature dependence of the Kondo peak ( $k_B T_K = 0.2$  meV), we find that the average induced gap is 4 times larger. In this device, the larger finite Andreev pair energy results in a doublet ground state where the radical's spin is not sufficiently screened by quasiparticle states near

the Fermi energy in the superconducting state to allow the Kondo singlet.

By applying a perpendicular magnetic field (see inset of fig. 3(a)), the ground state of the system can be tuned from the doublet ground state to the Kondo singlet. As the field is increased the Shiba peaks move to lower bias voltages, following the closure of the proximity-induced gaps. At a field of  $\approx 130$  mT the gap completely closes leaving a zero bias peak due to Kondo screening of the radical's spin and a phase transition to the Kondo-like singlet ground state.

Our low temperature measurements are further supported by calculations. Starting with a modified Anderson impurity model (Anderson Hamiltonian coupled to leads modeled by BCS Hamiltonians) we calculate the differential conductance as a function of bias voltage using the non-crossing approximation<sup>3,45,46</sup>. The broadening of the DOS due to the proximity effect is handled by introducing the Dynes function which is taken as a phenomenological broadening term that softens the BCS DOS of the bulk reservoirs<sup>3,47</sup>. Fig. 3(b) shows a conductance curve from this calculation where the main features of the experimental curve can be reproduced. A zero-bias peak is present when the order parameter in the leads is set to zero (red curve). In the superconducting state with  $\delta = 4T_K$  and broadening ( $0.15\delta$ ), two peaks can be seen with accompanying side dips and shoulders at higher and lower bias, respectively (black curve). Quantitative differences are primarily due to an asymmetry in the couplings ( $\Gamma_L/\Gamma_R$ ) discussed previously which reduces the Kondo peak from  $2e^2/h$  and the exact shape of the DOS for each gold lead. Differences in the lengths of the two gold leads (see Supporting information for details) means the broadening for the two leads would be different.

#### IV. GROUND STATE SPECTROSCOPY IN THE SUPERCONDUCTING STATE

Depending on the relative energies of the proximity-induced gap and the Kondo energy, the ground state of the system, even in the superconducting state, can take the form of a doublet for weak coupling ( $k_b T_K < \delta$ ) or a Kondo-like singlet for strong coupling ( $k_b T_K > \delta$ ). By virtue of a variable molecule-electrode coupling, we probe a large range of Kondo energies relative to the average induced gap energy. In the Supporting Information we show an overview of the 7 devices (A-G) having similar characteristics ordered by increasing Kondo

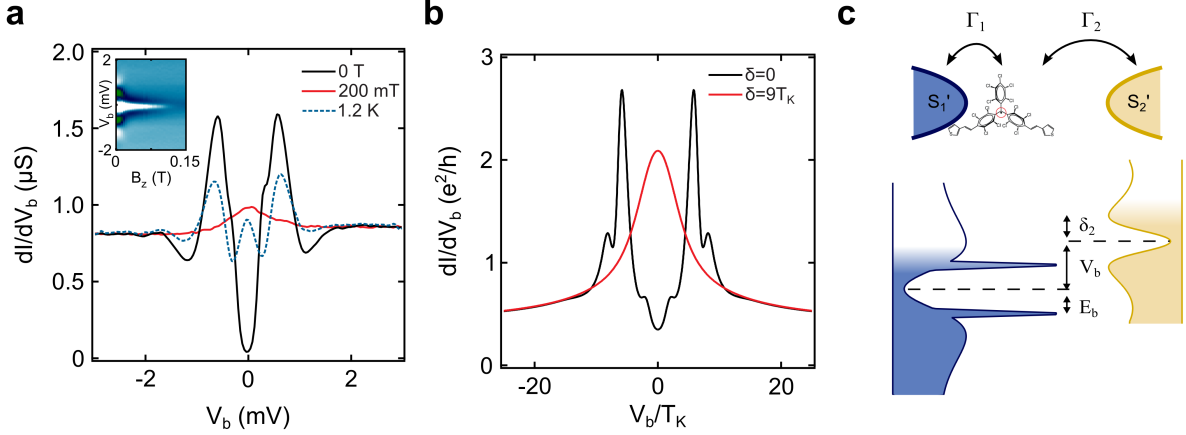


**FIG. 3. Characterization and calculations of a molecular junction in the superconducting state.** (a) Low temperature (100 mK) measurement of the differential conductance ( $dI/dV_b$ ) as a function of voltage bias ( $V_b$ ) of a radical molecular junction at zero magnetic field (superconducting state) and 200 mT (normal state). The blue dashed curve shows the same measurement at 1.2 K ( $B = 0$  T). The inset shows the magnetic field dependence of the Shiba peaks. (b) Theoretical calculations of the modeled system taking into account the proximity-induced DOS of the leads. (c) Schematic representation of the probing of the Shiba excited state as a result of the coupling of the radical molecule with the proximity-induced superconducting Au electrode.

energy. The Kondo temperature ranges from ( $\approx 1$  K to 18 K) for the seven devices.

In fig. 4 we show the weakest and strongest Kondo energy devices (junctions A and G). For junction A a Kondo peak cannot be discerned in the normal state (red curve fig. 4(a)) but a splitting ( $g = 2.1$ ) of the background is observed at higher magnetic fields fig. 4(b)). We estimate a Kondo temperature of  $\approx 1$  K from the critical field ( $B_c \approx 0.5k_bT_K/(g\mu_B)$ ) at which the background begins to split in fig. 4(b) ( $B_c \approx 0.36$  T). Following the analysis for device D above we estimate an average induced gap of 0.8 meV. Comparing the two energy scales (0.8 meV vs. 0.09 meV), this device is similar to device D in which the doublet ground state wins over the Kondo singlet. The inset of fig. 4(a) shows the calculations for this regime where we have taken  $\delta = 9T_K$  and built in an asymmetry of  $\Gamma_L/\Gamma_R = 20$  to better simulate the results. Shiba peaks in this regime correspond to singlet excitations of the doublet ground state. This situation is depicted in fig. 4(c) in the excitation picture where a thick barrier and reduced quasiparticle states near the Fermi energy prevent the Kondo singlet from claiming the ground state of the coupled system. Here we signify the

ground state and the excited state by occupancies of the molecule and the leads,  $|n_{mole}, n_{lead}\rangle$ . The Shiba excited state for this ground state,  $|\downarrow, \uparrow\rangle$ , is a singlet composed of the molecule's unpaired spin and an electron from a correlated Andreev pair in the leads (signified by the black arrow).

In fig. 4(d) we present the device with the largest Kondo temperature observed (18 K, estimated from the peak width). Comparing the characteristic energies for this device ( $\delta_{avg} = 0.7$  meV,  $k_b T_K = 1.6$  meV) we find that the large Kondo energy allows for screening of the radical's spin even in the superconducting state. This results in a singlet ground state at  $B = 0$  T. Calculations for this regime are shown in the inset of fig. 4(d) where we have taken  $\delta = 0.5T_K$  and a broadening of  $0.25\delta$ . Excitations of this ground state are the magnetic doublet. This is depicted in fig. 4(f) in the excitation picture. A weak barrier allows for screening from electrons in the proximity-induced leads and a singlet state is formed by the combination of the radical's spin and an electron in the leads.

## V. CONCLUSION

In conclusion, we have presented an investigation of the large- $U$  superconductor-QD phase diagram in the form of a radical molecule coupled to a proximity induced superconductor. In the superconducting state, we observe excitations which are characteristic of Shiba states as a result of the coupling between the radical and a proximity-induced superconductor. By applying a finite magnetic field, the proximity effect can be suppressed which allows a spin 1/2 Kondo effect. For the devices with the weakest and strongest Kondo energies we are able to probe both the doublet and singlet ground states which give rise to the singlet and doublet Shiba excited states, respectively. Our measurements are supported by calculations of the Anderson impurity model modified to account for the proximity-induced superconducting electrodes. Hybrid molecular junctions offer a unique investigation of the superconductor-QD system. In particular, with a suitable choice of molecule, an *in-situ* tunable Kondo effect would allow direct driving of the singlet to doublet quantum phase transition for a spin 1/2 impurity and the exact energies at which it occurs which is still an open question<sup>2,48,49</sup>.

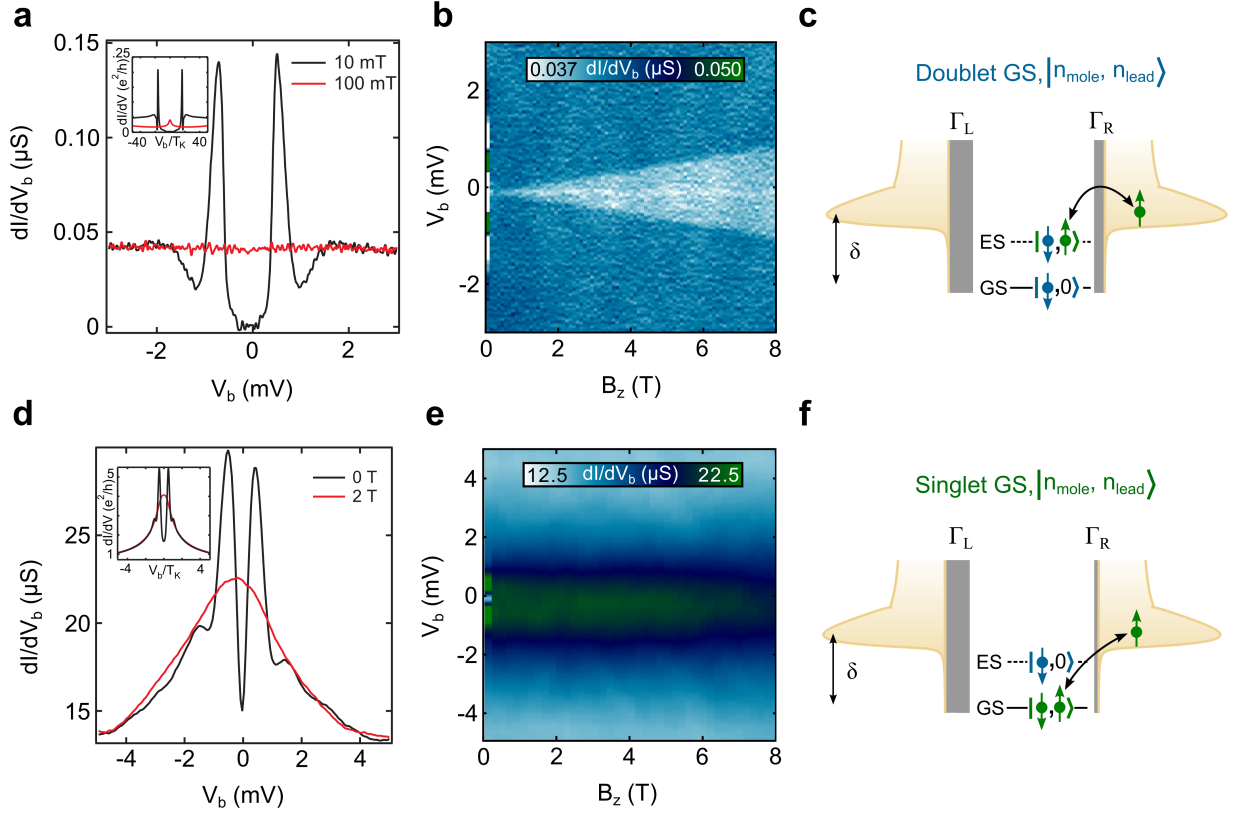


FIG. 4. **Ground state spectroscopy of the hybrid radical system.** (a) The differential conductance ( $dI/dV_b$ ) as a function of voltage bias ( $V_b$ ) of a radical molecular junction at zero magnetic field (superconducting state) and 200 mT (normal state) in the doublet ground state regime ( $T_K < \delta$ ). Inset shows calculations for this regime ( $\delta = 9T_K$ ). (b) Color plot of the differential conductance ( $dI/dV_b$ ) as a function of voltage bias and magnetic field for the junction in panel (a). (c) Excitation picture of the ground and excited states in the doublet ground state regime. (d) The differential conductance ( $dI/dV_b$ ) as a function of voltage bias ( $V_b$ ) of a radical molecular junction at zero magnetic field (superconducting state) and 2 T (normal state) in the singlet ground state regime ( $T_K > \delta$ ). Inset shows calculations for this regime ( $\delta = 0.5T_K$ ). (e) Color plot of the differential conductance ( $dI/dV_b$ ) as a function of voltage bias and magnetic field for the junction in panel (d). (f) Excitation picture of the ground and excited states in the singlet ground state regime.



## VI. ACKNOWLEDGMENTS

The authors acknowledge financial support by the Dutch Organization for Fundamental research (FOM), the Ministry of Education, Culture, and Science (OCW), the Netherlands Organization for Scientific Research (NWO), and an ERC advanced grant (MolS@MolS). C.F., M.M.-T., C.R. and J.V. acknowledge the financial support from Spanish Ministry of Economy and Competitiveness, through the DGI (CTQ2013-40480-R) and Severo Ochoa Programme for Centres of Excellence in R&D (SEV-2015-0496), the Generalitat de Catalunya (2014SGR-17) and the Networking Research Center of Bioengineering, Biomaterials and Nanomedicine (CIBER-BBN). C.F. is enrolled in the Materials Science PhD program of UAB. T.M.K. acknowledges the support from the European Research Council Advanced Grant No. 339306 (METIQUM) and from the Ministry of Education and Science of the Russian Federation, Contract No. 14.B25.31.0007. R.A. acknowledges grants FIS2012-33521 and FIS-2015-64654 (MINECO/FEDER).

**Competing financial interests** The authors declare no competing financial interests.

## VII. AUTHOR CONTRIBUTIONS

J.O.I. conceived the experiment. C.F., M.M.-T., C.R. and J.V. synthesized the molecule. J.O.I. and R.G. fabricated the devices and performed the experiments. J.O.I., R.G., J.dB., E.B., and T.M.K. performed data analysis and interpretation. R.A. performed the calculations. J.O.I. wrote the manuscript with significant contributions from all authors. H.S.J.vdZ. oversaw experiments and advised on data interpretation.

## REFERENCES

- <sup>1</sup>Silvano De Franceschi, Leo Kouwenhoven, Christian Schönenberger, and Wolfgang Wernsdorfer. Hybrid superconductor-quantum dot devices. *Nature Nanotechnology*, 5(10):703–711, 2010.
- <sup>2</sup>KJ Franke, G Schulze, and JI Pascual. Competition of superconducting phenomena and kondo screening at the nanoscale. *Science*, 332(6032):940–944, 2011.

- <sup>3</sup>Eduardo JH Lee, Xiaocheng Jiang, Ramón Aguado, Georgios Katsaros, Charles M Lieber, and Silvano De Franceschi. Zero-bias anomaly in a nanowire quantum dot coupled to superconductors. *Physical Review Letters*, 109(18):186802, 2012.
- <sup>4</sup>W Chang, VE Manucharyan, Thomas Sand Jespersen, Jesper Nygård, and Charles M Marcus. Tunneling spectroscopy of quasiparticle bound states in a spinful josephson junction. *Physical Review Letters*, 110(21):217005, 2013.
- <sup>5</sup>Eduardo JH Lee, Xiaocheng Jiang, Manuel Houzet, Ramón Aguado, Charles M Lieber, and Silvano De Franceschi. Spin-resolved andreev levels and parity crossings in hybrid superconductor-semiconductor nanostructures. *Nature nanotechnology*, 9(1):79–84, 2014.
- <sup>6</sup>Jong Soo Lim, Rosa López, Ramón Aguado, et al. Shiba states and zero-bias anomalies in the hybrid normal-superconductor anderson model. *Physical Review B*, 91(4):045441, 2015.
- <sup>7</sup>Nino Hatter, Benjamin W Heinrich, Michael Ruby, Jose I Pascual, and Katharina J Franke. Magnetic anisotropy in shiba bound states across a quantum phase transition. *Nature communications*, 6:8988, 2015.
- <sup>8</sup>Martin Žonda, Vladislav Pokorný, Václav Janiš, and Tomáš Novotný. Perturbation theory for an anderson quantum dot asymmetrically attached to two superconducting leads. *Physical Review B*, 93(2):024523, 2016.
- <sup>9</sup>Michael Ruby, Falko Pientka, Yang Peng, Felix von Oppen, Benjamin W Heinrich, and Katharina J Franke. Tunneling processes into localized subgap states in superconductors. *Physical Review Letters*, 115(8):087001, 2015.
- <sup>10</sup>JD Pillet, CHL Quay, P Morfin, C Bena, A Levy Yeyati, and P Joyez. Andreev bound states in supercurrent-carrying carbon nanotubes revealed. *Nature Physics*, 6(12):965–969, 2010.
- <sup>11</sup>J-D Pillet, P Joyez, MF Goffman, et al. Tunneling spectroscopy of a single quantum dot coupled to a superconductor: From kondo ridge to andreev bound states. *Physical Review B*, 88(4):045101, 2013.
- <sup>12</sup>Vincent Mourik, Kun Zuo, Sergey M Frolov, SR Plissard, EPAM Bakkers, and LP Kouwenhoven. Signatures of majorana fermions in hybrid superconductor-semiconductor nanowire devices. *Science*, 336(6084):1003–1007, 2012.
- <sup>13</sup>W Chang, SM Albrecht, TS Jespersen, Ferdinand Kuemmeth, P Krogstrup, J Nygård, and CM Marcus. Hard gap in epitaxial semiconductor–superconductor nanowires. *Nature*

- nanotechnology*, 10(3):232–236, 2015.
- <sup>14</sup>Tobias Meng, Serge Florens, and Pascal Simon. Self-consistent description of andreev bound states in josephson quantum dot devices. *Physical Review B*, 79(22):224521, 2009.
- <sup>15</sup>L Yu. Bound state in superconductors with paramagnetic impurities. *Acta Phys. Sin*, 21:75–91, 1965.
- <sup>16</sup>Hiroyuki Shiba. Classical spins in superconductors. *Progress of theoretical Physics*, 40(3):435–451, 1968.
- <sup>17</sup>AI Rusinov. Superconductivity near a paramagnetic impurity. *Soviet Journal of Experimental and Theoretical Physics Letters*, 9:85, 1969.
- <sup>18</sup>AV Balatsky, I Vekhter, and Jian-Xin Zhu. Impurity-induced states in conventional and unconventional superconductors. *Reviews of Modern Physics*, 78(2):373, 2006.
- <sup>19</sup>Ali Yazdani, BA Jones, CP Lutz, MF Crommie, and DM Eigler. Probing the local effects of magnetic impurities on superconductivity. *Science*, 275(5307):1767–1770, 1997.
- <sup>20</sup>S Nadj-Perge, IK Drozdov, BA Bernevig, and Ali Yazdani. Proposal for realizing majorana fermions in chains of magnetic atoms on a superconductor. *Physical Review B*, 88(2):020407, 2013.
- <sup>21</sup>Falko Pientka, Leonid I Glazman, and Felix von Oppen. Topological superconducting phase in helical shiba chains. *Physical Review B*, 88(15):155420, 2013.
- <sup>22</sup>Stevan Nadj-Perge, Ilya K Drozdov, Jian Li, Hua Chen, Sangjun Jeon, Jungpil Seo, Allan H MacDonald, B Andrei Bernevig, and Ali Yazdani. Observation of majorana fermions in ferromagnetic atomic chains on a superconductor. *Science*, 346(6209):602–607, 2014.
- <sup>23</sup>L Dumoulin, E Guyon, and P Nedellec. Tunneling study of localized bands in superconductors with magnetic impurities (normal kondo alloys in the superconducting proximity). *Physical Review B*, 16(3):1086, 1977.
- <sup>24</sup>Gerbold C Ménard, Sébastien Guissart, Christophe Brun, Stéphane Pons, Vasily S Stolyarov, François Debontridder, Matthieu V Leclerc, Etienne Janod, Laurent Cario, Dimitri Roditchev, et al. Coherent long-range magnetic bound states in a superconductor. *Nature Physics*, 11(12):1013–1016, 2015.
- <sup>25</sup>Brian Møller Andersen, Karsten Flensberg, Verena Koerting, and Jens Paaske. Nonequilibrium transport through a spinful quantum dot with superconducting leads. *Physical Review Letters*, 107(25):256802, 2011.

- <sup>26</sup>Bum-Kyu Kim, Ye-Hwan Ahn, Ju-Jin Kim, Mahn-Soo Choi, Myung-Ho Bae, Kicheon Kang, Jong Soo Lim, Rosa López, and Nam Kim. Transport measurement of andreev bound states in a kondo-correlated quantum dot. *Physical Review Letters*, 110(7):076803, 2013.
- <sup>27</sup>A Kumar, M Gaim, D Steininger, A Levy Yeyati, A Martín-Rodero, AK Hüttel, and C Strunk. Temperature dependence of andreev spectra in a superconducting carbon nanotube quantum dot. *Physical Review B*, 89(7):075428, 2014.
- <sup>28</sup>A Yu Kitaev. Unpaired majorana fermions in quantum wires. *Physics-Uspekhi*, 44(10S):131, 2001.
- <sup>29</sup>Jason Alicea. Majorana fermions in a tunable semiconductor device. *Physical Review B*, 81(12):125318, 2010.
- <sup>30</sup>Jay D Sau, Roman M Lutchyn, Sumanta Tewari, and S Das Sarma. Generic new platform for topological quantum computation using semiconductor heterostructures. *Physical review letters*, 104(4):040502, 2010.
- <sup>31</sup>Yuval Oreg, Gil Refael, and Felix von Oppen. Helical liquids and majorana bound states in quantum wires. *Physical review letters*, 105(17):177002, 2010.
- <sup>32</sup>Jason Alicea. New directions in the pursuit of majorana fermions in solid state systems. *Reports on Progress in Physics*, 75(7):076501, 2012.
- <sup>33</sup>SM Albrecht, AP Higginbotham, M Madsen, F Kuemmeth, TS Jespersen, Jesper Nygård, P Krogstrup, and CM Marcus. Exponential protection of zero modes in majorana islands. *Nature*, 531(7593):206–209, 2016.
- <sup>34</sup>Clemens B Winkelmann, Nicolas Roch, Wolfgang Wernsdorfer, Vincent Bouchiat, and Franck Balestro. Superconductivity in a single-c60 transistor. *Nature Physics*, 5(12):876–879, 2009.
- <sup>35</sup>Kang Luo and Zhen Yao. Fabrication of nanometer-spaced superconducting pb electrodes. *Applied Physics Letters*, 95(11):113115, 2009.
- <sup>36</sup>AF Andreev. The thermal conductivity of the intermediate state in superconductors. *Soviet Physics JETP*, 19(5):1823, 1964.
- <sup>37</sup>Riccardo Frisenda, Rocco Gaudenzi, Carlos Franco, Marta Mas-Torrent, Concepció Rovira, Jaume Veciana, Isaac Alcon, Stefan T Bromley, Enrique Burzurí, and Herre SJ Van der Zant. Kondo effect in a neutral and stable all organic radical single molecule break junction. *Nano letters*, 15(5):3109–3114, 2015.

- <sup>38</sup>Manuel Ballester. Inert free radicals (ifr): a unique trivalent carbon species. *Accounts of Chemical Research*, 18(12):380–387, 1985.
- <sup>39</sup>R Gaudenzi, JO Island, J De Bruijkere, E Burzurí, TM Klapwijk, and HSJ Van der Zant. Superconducting molybdenum-rhenium electrodes for single-molecule transport studies. *Applied Physics Letters*, 106(22):222602, 2015.
- <sup>40</sup>K ONeill, EA Osorio, and HSJ Van der Zant. Self-breaking in planar few-atom au constrictions for nanometer-spaced electrodes. *Applied Physics Letters*, 90(13):133109, 2007.
- <sup>41</sup>Michael Wolz, Christian Debuschewitz, Wolfgang Belzig, and Elke Scheer. Evidence for attractive pair interaction in diffusive gold films deduced from studies of the superconducting proximity effect with aluminum. *Physical Review B*, 84(10):104516, 2011.
- <sup>42</sup>Wolfgang Belzig, Christoph Bruder, and Gerd Schön. Local density of states in a dirty normal metal connected to a superconductor. *Physical Review B*, 54(13):9443, 1996.
- <sup>43</sup>JJ Parks, AR Champagne, GR Hutchison, S Flores-Torres, HD Abruna, and DC Ralph. Tuning the kondo effect with a mechanically controllable break junction. *Physical Review Letters*, 99(2):026601, 2007.
- <sup>44</sup>TA Costi, AC Hewson, and V Zlatic. Transport coefficients of the anderson model via the numerical renormalization group. *Journal of Physics: Condensed Matter*, 6(13):2519, 1994.
- <sup>45</sup>Aashish A Clerk and Vinay Ambegaokar. Loss of  $\pi$ -junction behavior in an interacting impurity josephson junction. *Physical Review B*, 61(13):9109, 2000.
- <sup>46</sup>Gabriel Sellier, Thilo Kopp, Johann Kroha, and Yuri S Barash.  $\pi$  junction behavior and andreev bound states in kondo quantum dots with superconducting leads. *Physical Review B*, 72(17):174502, 2005.
- <sup>47</sup>RC Dynes, V Narayanamurti, and J Pm Garno. Direct measurement of quasiparticle-lifetime broadening in a strong-coupled superconductor. *Physical Review Letters*, 41(21):1509, 1978.
- <sup>48</sup>Tamifusa Matsuura. The effects of impurities on superconductors with kondo effect. *Progress of Theoretical Physics*, 57(6):1823–1835, 1977.
- <sup>49</sup>Osamu Sakai, Yukihiro Shimizu, Hiroyuki Shiba, and Koji Satori. Numerical renormalization group study of magnetic impurities in superconductors. ii. dynamical excitation spectra and spatial variation of the order parameter. *Journal of the Physical Society of Japan*, 62(9):3181–3197, 1993.

# Supporting Information: Proximity-induced Shiba states in a molecular junction

## I. LOW TEMPERATURE CHARACTERISTICS OF EMPTY GAPS

Fig. S1 shows low-temperature characteristics for another empty gap in addition to the one presented in the main text in fig. 2(a). Fig. S1(a) shows the differential conductance ( $dI/dV$ ) as a function of the voltage bias ( $V_b$ ) in the superconducting state ( $B = 0$  T) and the normal state ( $B = 200$  mT). Fig. S1(b) shows  $dI/dV$  as a function of  $V_b$  and magnetic field. The critical field of the proximity induced superconductivity is roughly around 200 mT. Fig. S1(c) shows a scanning electron microscopy image of the junction after measurement. The difference in the length of the left and right electrode results in stronger and weaker proximity effects, respectively. Additionally, the shape of the electrode will play a role in the overall density of states of the proximity induced leads. In the normal state however, none of the empty gaps show the presence of a zero-bias peak in the low temperature characteristics that would signify Kondo screening of an impurity.

## II. DEVICE OVERVIEW

Fig. S2 shows an overview of all 7 junctions measured showing symmetric conductance peaks in the superconducting state and a zero-bias peak in the normal state. From the top to the bottom, the devices are arranged according to their critical field  $B_c$  of the Kondo peak except for device G which does not show a splitting because the critical field is larger than our experimental range. All devices were measured at  $\approx 100$  mK except for devices E and F which were measured at 1.8 K. The left side panels in fig. S2 shows the differential conductance  $dI/dV_b$  as a function of voltage bias  $V_b$  for each device in the superconducting state (0 T, black curve) and the normal state (200 mT, red curve). The right side panels show  $dI/dV_b$  as a function of  $V_b$  and magnetic field.

## III. GATE DEPENDENCE

We observe little modulation of the conductance with back gate voltage due to the sizable (2 eV) SOMO-LUMO gap of the radical molecule. Fig. S3(a) shows  $dI/dV$  as a function

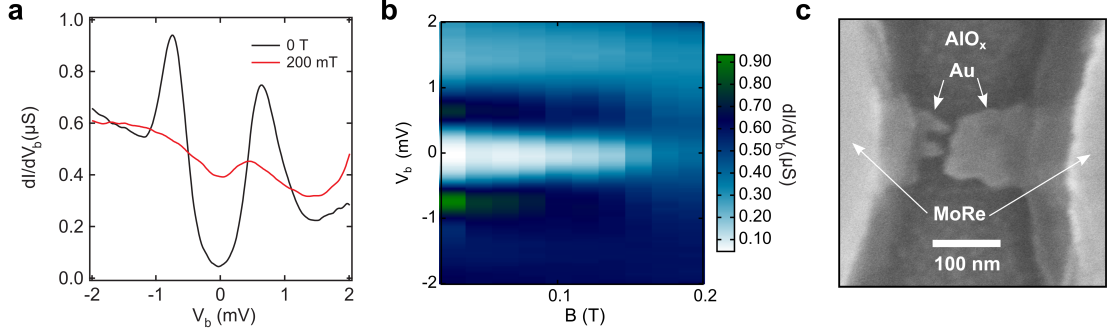


FIG. S1. **Characteristics of another empty gap measured at low-temperature.** (a) Numerical differential conductance ( $dI/dV_b$ ) as a function of voltage bias ( $V_b$ ). The black curve shows the measurement at zero field and the red curve shows the measurement near the critical field of the proximity induced superconductivity. (b) Color plot of  $dI/dV_b$  as a function of  $V_b$  and perpendicular magnetic field. (c) Scanning electron microscopy image of the junction after measurement.

of  $V_b$  and  $V_g$  for device E. With our accessible gate range, no degeneracy point is reached that would signal a shift to another charge state. The same is true in the normal state (see Fig. S3(b)). In fact, very little modulation of the conductance is observed (see Fig. S3(c)) overall which supports the robust Kondo effect and stable spin 1/2 nature of the molecule.

#### IV. TEMPERATURE DEPENDENCE OF THE ANOMALOUS ZERO-BIAS PEAKS

At finite temperatures ( $\sim 1$  K) a zero-bias peak emerges in the conductance curves which grows with temperature. Devices E and F show the presence of a zero-bias peak (see Device overview section). Zero bias peaks also emerge for devices A and D at higher temperatures (see Fig. S4). A plausible explanation for this peak is that a mini Kondo peak emerges in the gap at higher quasiparticle filling. Further supporting this claim is Fig. S4(c) which shows calculated curves of the modified Anderson impurity model (see main text for details) as a function of increased quasiparticle broadening in the leads. Similar to an increase of quasiparticles at higher temperatures, increased broadening leads to a zero-bias peak.

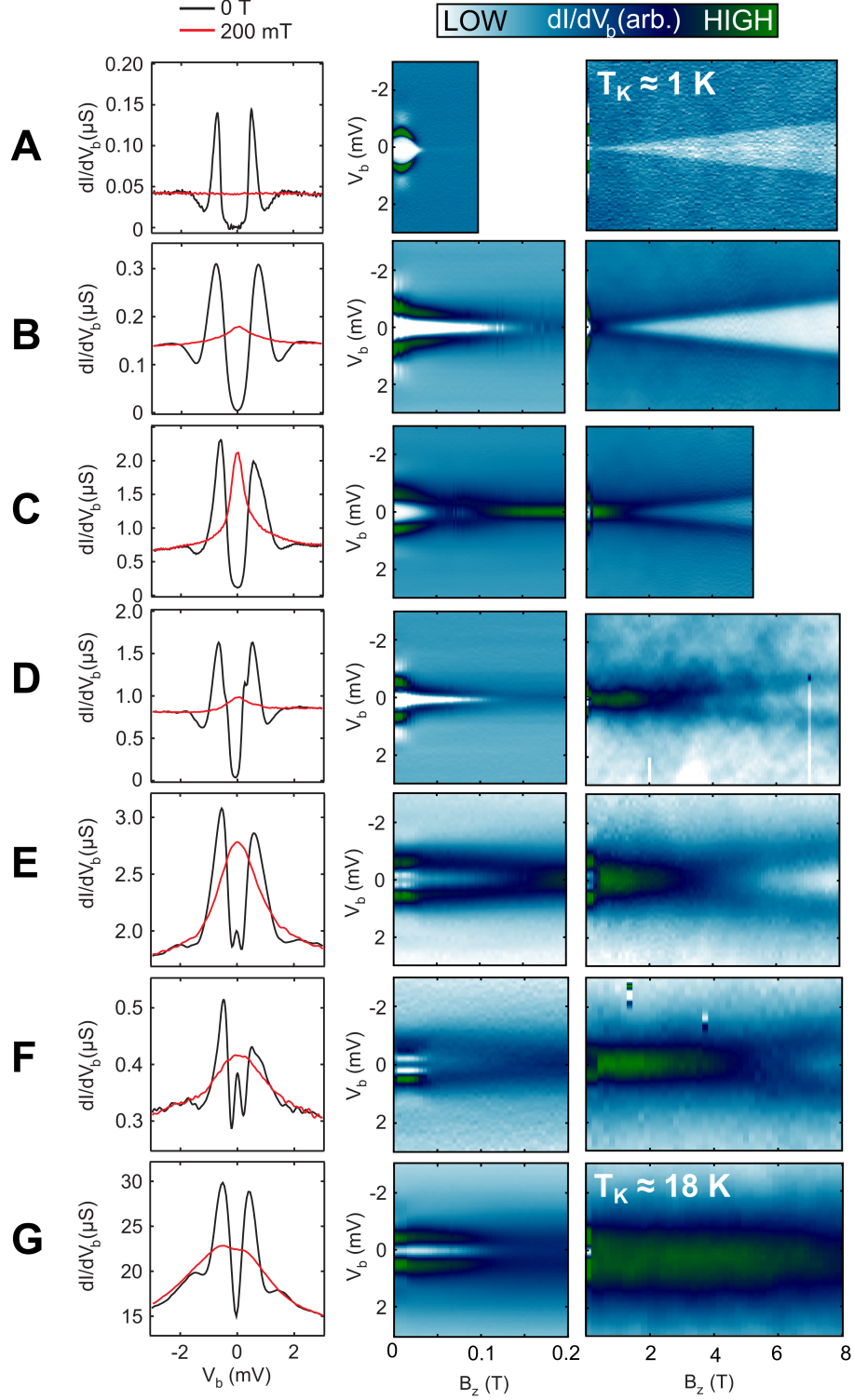


FIG. S2. **Overview of all 7 devices measured.** The left-side panels show  $dI/dV_b$  as a function of  $V_b$  and the right-side panels show color plots of  $dI/dV_b$  as a function of  $V_b$  and magnetic field applied perpendicular to the junction.



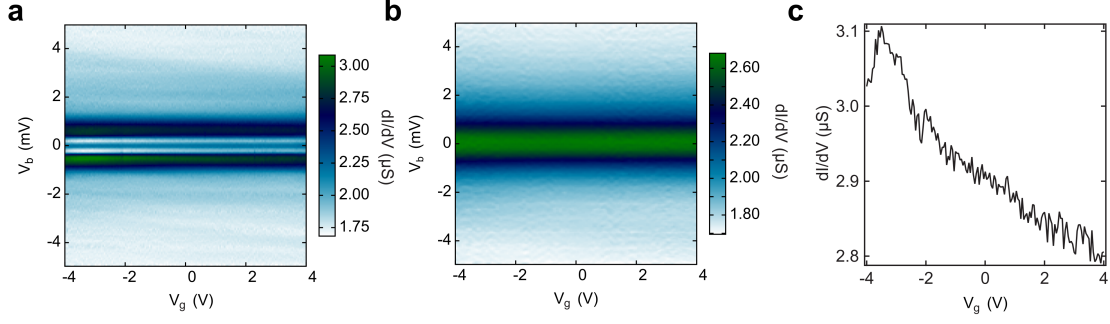


FIG. S3. **Gate dependence** (a) A color plot of the  $dI/dV$  as a function of  $V_b$  and  $V_g$  in the superconducting state ( $B = 0$  T). (b) A color plot of the  $dI/dV$  as a function of  $V_b$  and  $V_g$  in the normal state ( $B = 300$  mT). (c) Line cut from panel (a) at a voltage of  $V_b = -0.5$  mV showing a small modulation with gate voltage.

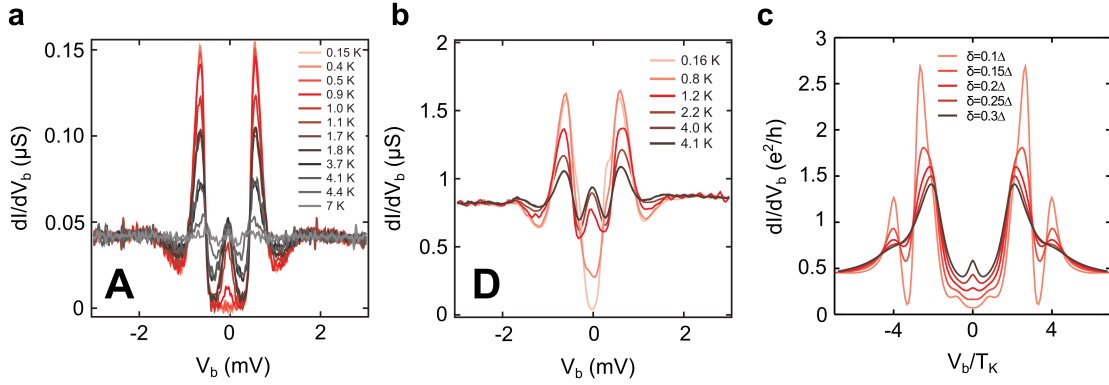


FIG. S4. **Temperature dependence of the anomalous zero-bias peak** (a)  $dI/dV$  as a function of  $V_b$  for sample A as a function of temperature. (b)  $dI/dV$  as a function of  $V_b$  for sample D as a function of temperature. (c) Calculations of conductance as a function of  $V_b$  for increasing phenomenological broadening ( $\delta$ ) of the BCS gap.